Published in final edited form as:
Respir Physiol Neurobiol. 2012 January 15; 180(1): 88–96. doi:10.1016/j.resp.2011.10.015.

Structure-Activity Relationships in Rodent Diaphragm Muscle Fibers vs. Neuromuscular Junctions

Dylan C. Sieck[a], **Wen-Zhi Zhan**[b], **Yun-Hua Fang**[b], **Leonid G. Ermilov**[b], **Gary C. Sieck**[a,b], and **Carlos B. Mantilla**[a,b,*]

[a]Department of Anesthesiology, College of Medicine, Mayo Clinic, 200 First St. SW, Rochester MN 55905, USA

[b]Department of Physiology & Biomedical Engineering, College of Medicine, Mayo Clinic, 200 First St. SW, Rochester MN 55905, USA

Abstract

The diaphragm muscle (DIAm) is a highly active muscle of mixed fiber type composition. We hypothesized that consistent with greater activation history and proportion of fatigue-resistant fibers, neuromuscular transmission failure is lower in the mouse compared to the rat DIAm, and that neuromuscular junction (NMJ) morphology will match their different functional demands. Minute ventilation and duty cycle were higher in the mouse than in the rat. The proportion of fatigue-resistant fibers was similar in the rat and mouse; however the contribution of fatigue-resistant fibers to total DIAm mass was higher in the mouse. Neuromuscular transmission failure was less in mice than in rats. Motor end-plate area differed across fibers in rat but not in mouse DIAm, where NMJs displayed greater complexity overall. Thus, differences across species in activation history and susceptibility to neuromuscular transmission failure are reflected in the relative contribution of fatigue resistant muscle fibers to total DIAm mass, but not in type-dependent morphological differences at the NMJ.

Keywords

Motor unit; plethysmography; morphometry; respiratory muscles; fiber type

1. Introduction

Within the diaphragm muscle (DIAm), the properties of a phrenic motor neuron and the muscle fibers it innervates are matched to comprise a motor unit (Enad et al., 1989; Fournier and Sieck, 1988; Sieck, 1988; Sieck et al., 1989a; Sieck et al., 1996). Diaphragm motor units are selectively recruited to accomplish different ventilatory and non-ventilatory behaviors such that fatigue-resistant motor units are recruited during sustained ventilatory behaviors while more fatigable units are recruited during the shorter-duration, higher-force non-ventilatory behaviors involved in airway clearance (e.g., coughing, sneezing) (Fournier and Sieck, 1988; Mantilla et al., 2010; Mantilla and Sieck, 2011; Sieck, 1991; Sieck and

*Corresponding Author: Carlos B. Mantilla, M.D., Ph.D., Tel: +1 (507) 255-7481, Fax: +1 (507) 255-7300, mantilla.carlos@mayo.edu.

Fournier, 1989). Forces generated by the DIAm to accomplish quiet breathing (i.e., eupnea) represent ~27% of maximal force (transdiaphragmatic pressure generated by bilateral supramaximal phrenic nerve stimulation) in rats (Mantilla et al., 2010), ~17% in cats (Fournier and Sieck, 1988; Sieck and Fournier, 1989) and ~10% in humans (Sieck, 1991). This scaling across species is consistent with the scaling of other ventilatory parameters such as tidal volume (V_T), total lung capacity and ventilation ($\dot{V}_E$) (Lindstedt and Schaeffer, 2002; Stahl, 1967). Respiratory rate and inspiratory duty cycle also increase as animal size decreases. This scaling of ventilatory requirements generally matches the distribution of DIAm motor unit (muscle fiber) types across these species (Fournier and Sieck, 1988; Mantilla et al., 2010; Mantilla and Sieck, 2011; Sieck, 1991, 1995; Sieck and Fournier, 1989). Accordingly, the proportion of type I and IIa fibers (comprising fatigue-resistant motor units) across species is also scaled to match the fractional motor unit recruitment that is necessary to accomplish sustained ventilatory behaviors (Mantilla and Sieck, 2011).

In the rat DIAm, neuromuscular junction (NMJ) morphology varies across motor unit (muscle fiber) types (Mantilla et al., 2004a; Prakash et al., 1996b; Rowley et al., 2007; Sieck and Prakash, 1997). For example, NMJs at type I and IIa fibers are smaller and less complex compared to NMJs at type IIx and/or IIb fibers. This suggests that NMJ morphology is matched to the functional demands of different motor unit types. Indeed, susceptibility to neuromuscular transmission failure varies across motor unit (muscle fiber) types (Ermilov et al., 2007; Johnson and Sieck, 1993; Kugelberg and Lindegren, 1979). In the rat DIAm, the safety factor for neuromuscular transmission is higher at type IIx and/or IIb fibers compared to type I or IIa fibers (Ermilov et al., 2007; Wood and Slater, 1997, 2001). However, with repetitive stimulation, quantal release at type IIx and/or IIb fibers declines far more rapidly than at type I or IIa fibers (Reid et al., 1999; Rowley et al., 2007) providing a basis for the demonstrated greater susceptibility for neuromuscular transmission failure at these fibers (Johnson and Sieck, 1993; Sieck and Prakash, 1995).

Given the scaling of ventilatory parameters that has been demonstrated across species, we hypothesized that because of the mouse DIAm is more active (prolonged inspiratory duty cycle and greater weight-adjusted ventilation) than the rat, the mouse DIAm will have: 1) greater relative proportion of fatigue-resistant motor units (type I or IIa fibers); and, 2) reduced susceptibility to neuromuscular transmission failure. We also hypothesized that NMJ morphology in the mouse DIAm will be matched to the functional demands of different motor unit types.

2. Methods

Adult male Sprague Dawley rats (body weight ~300 g) and adult male C57BL/6J mice (body weight ~25 g) were used in these experiments. All procedures were approved by the Institutional Animal Care and Use Committee.

2.1. Assessment of ventilatory parameters

In a subset of rats (n = 10) and mice (n = 9), ventilatory parameters including V_T, VE, ventilatory frequency, inspiratory and expiratory durations and inspiratory duty cycle were recorded using a whole body plethysmography system (Buxco Inc., Wilmington, NC). Prior to each recording, a calibration procedure was performed according to the manufacturer's recommendations. Ventilatory parameters during resting, awake conditions were measured after ~5 min of acclimatization when stable respiratory patterns were observed. If stability had not been reached, a longer period of acclimatization was allowed. Afterwards, ventilatory parameters were recorded for 10–12 min.

2.2. Assessment of muscle fiber type proportions and cross-sectional areas

In a subset of rats and mice (n=6 each), the proportion and fiber cross-sectional area (CSA) was determined at type-identified muscle fibers. Animals were euthanized by exsanguination under deep levels of anesthesia induced by intramuscular injection of ketamine (90 mg/kg) and xylazine (10 mg/kg). The DIAm was exposed via a laparotomy, quickly excised and pinned on cork at 1.5 times resting length (which approximates optimal length, L_o; Zhan et al., 1997). As in previous studies (LaBella et al., 1998; Miyata et al., 1995; Prakash et al., 2000; Zhan et al., 1997), the whole DIAm was rapidly frozen in melting isopentane and five serial sections (10 μm thick) were cut along the fiber short-axis using a cryostat. Briefly, sections were incubated with primary antibodies against the different MyHC isoforms: anti-$MyHC_{Slow}$ (Novocastra, Wetzlar, Germany), anti-$MyHC_{2A}$ (A4.74 or N1.551), anti-$MyHC_{2B}$ (BF-F3) as well as an antibody reactive against all MyHC isoforms but $MyHC_{2X}$ (BF-35, all from Developmental Studies Hybridoma Bank – DSHB, Iowa City, IA). Sections were reacted with appropriate Cy3- or Cy5- conjugated secondary antibodies (Jackson ImmunoResearch Laboratories Inc., West Grove, PA) so that double labeling of MyHC isoforms was possible in the same section. The specificity of these primary antibodies has been previously validated (Zhan et al., 1997). Sections were covered in GelMount (Sigma-Aldrich Corp., St. Louis, MO) and imaged with an Olympus FluoView 300 laser scanning confocal microscope (Olympus America Inc., Melville, NY) mounted on an upright Olympus BX50WI microscope and equipped with Argon (488 nm) and HeNe (543 nm and 643 nm) lasers.

Digital images were obtained using an Olympus UApo 40x /340 (1.35 NA) oil-immersion objective. As previously reported (Prakash et al., 2000; Prakash et al., 1996b; Prakash et al., 1993, 1994; Sieck et al., 1999a), optical resolution was empirically determined for the acquisition conditions in all experiments using 4 μm yellow-green (488 nm) fluorescent latex FluoSpheres (Invitrogen). Accordingly, pixel dimensions in the 800×600 acquisition array (0.5 × 0.5 μm pixels) were set to be slightly above the optical resolution for the lens, avoiding oversampling. DIAm sections treated identically but lacking the corresponding primary antibodies were used to adjust tissue background autofluorescence to <10% of the dynamic range. A single image was obtained per DIAm section. Fibers were then manually counted using MetaMorph software (Universal Imaging Corp., Downingtown PA). DIAm fiber proportions and dimensions were determined as previously described (Lewis et al., 1986; Miyata et al., 1995; Prakash et al., 2000; Sieck and Blanco, 1991; Sieck et al., 1989b; Zhan et al., 1997). On average, 580 fibers were counted per DIAm to determine the proportion of fibers of each type in all animals. The integrated morphometry tool was used to determine fiber CSA for each individually traced fiber; ~30 fibers of each type were measured in all animals.

2.3. Assessment of neuromuscular transmission failure

The extent of DIAm neuromuscular transmission failure was estimated in a subset of rats (n=6) and mice (n=8) using a previously described method (Aldrich et al., 1986; Ermilov et al., 2010; Fournier et al., 1991; Johnson and Sieck, 1993; Kuei et al., 1990; Mantilla et al., 2004b; Miyata et al., 1995; Prakash et al., 1999). Briefly, a segment of the midcostal region of the DIAm that included the phrenic nerve was mounted in a tissue bath containing Rees-Simpson solution (with the following composition in mM: Na^+ 135, K^+ 5, Ca^{2+} 2, Mg^{2+} 1, Cl^- 120, HCO_3^- 25 at pH 7.4) maintained at 26°C and oxygenated with 95% O_2 and 5% CO_2. The central tendon was attached to a force transducer (model 6350, Cambridge Technology, Cambridge, MA), while the rib insertion was clamped with a micromanipulator. Muscle length was adjusted to obtain maximal isometric twitch force in response to 1-ms monophasic rectangular pulses (L_o). To assess the extent of neuromuscular transmission failure, the phrenic nerve was stimulated using a suction electrode (0.2-ms

pulses in 40 Hz in 330-ms duration trains every 1 s for 2 min). Every 15 s, a single 40 Hz, 330-ms duration train was applied to the muscle using plate electrodes. The relative contribution of neuromuscular transmission failure to muscle fatigue was estimated as: *(NF-MF)/(1-MF)*, where *NF* is a percent decrement in force during repetitive nerve stimulation and *MF* is the percent force decrement during direct muscle stimulation.

Muscle fatigue resistance was also determined using separate DIAm segments. Repetitive stimulation of the DIAm (40 Hz, 330-ms trains, repeated every s) was used to calculate the ratio of force generated after 2 min of stimulation compared to the initial force (Aldrich et al., 1986; Ermilov et al., 2010; Mantilla et al., 2004b; Miyata et al., 1995; Prakash et al., 1999).

2.4. Assessment of NMJ morphology

The morphology of DIAm motor end-plates was measured in a subset of rats and mice (n=6 each). Motor end-plates were labeled by incubating DIAm samples with Alexa Fluor 488-conjugated α-bungarotoxin (0.1 μg/ml; Invitrogen Corp., Carlsbad, CA) after which samples were fixed with 2% paraformaldehyde. DIAm samples were incubated with an isoform-specific primary antibody to MyHC isoforms $MyHC_{Slow}$ and $MyHC_{2A}$ (N2-261, DSHB) followed by a Cy3-conjugated secondary antibody. Samples were pinned onto a silicon rubber (Sylgard; DowCorning, Midland, MI)-coated Petri dish before imaging. Although small differences in planar area were reported between NMJs at type I and IIa fibers in rat DIAm (Prakash et al., 1996b; Sieck et al., 1999b), subsequent studies did not verify these differences (Mantilla et al., 2004a; Prakash et al., 1996a; Prakash et al., 1999; Prakash et al., 1995; Sieck and Prakash, 1997). However, significant differences in NMJ planar area and branching were consistently observed between NMJs at type I and IIa fibers (expressing $MyHC_{Slow}$ or $MyHC_{2A}$, respectively) compared to type IIx and/or IIb fibers in the rat DIAm (expressing $MyHC_{2X}$ and/or $MyHC_{2B}$) (Ermilov et al., 2007; Mantilla et al., 2004a; Mantilla et al., 2007; Prakash et al., 1996a; Prakash et al., 1996b; Prakash et al., 1999; Prakash et al., 1995; Rowley et al., 2007; Sieck and Prakash, 1997; Sieck et al., 1999b). Thus, in the present study we compared morphological measurements in two groups: NMJs at type I and IIa vs. NMJs at type IIx and/or IIb fibers.

Confocal microscopy was used for morphological analyses of NMJ morphology as previously described (Mantilla et al., 2007; Prakash et al., 1993, 1994; Sieck et al., 1999a). Pixel dimensions (0.33 × 0.33 μm) were set to be above the optical resolution for this lens, avoiding oversampling. Two-channel registration was verified empirically using multicolor fluorescent beads (Invitrogen), as previously reported (Prakash et al., 1996b; Sieck et al., 1999a). The Z-axis resolution was also empirically determined from image stacks reconstructed in XZ, as previously reported (Sieck et al., 1999a). Step size was set to match the Z-axis resolution (0.8 μm), and sequential images were obtained stepping in only one direction to avoid issues with hysteresis in the stepper motor. Image stacks usually consisted of 8–10 images for each NMJ.

Motor end-plates labeled by Alexa Fluor 488-α-bungarotoxin and Cy3-labeled type I or IIa DIAm fibers were imaged simultaneously in two channels. Tissue autofluorescence levels were set to <10% of the dynamic range using separate DIAm samples, processed identically but without addition of fluorescently-labeled α-bungarotoxin or MyHC primary antibody.

Individual DIAm NMJs were visualized only on the surface of the thoracic side of the DIAm. Confocal image stacks were obtained from NMJs located superficially (usually within 50 μm of the surface) and “en face” in order to minimize fluorescence dispersion and to reduce the impact of anisotropic voxel dimensions on image reconstruction. Superficially located NMJs are not morphologically different from other NMJs located at great depths in

midcostal region of the rat DIAm (Mantilla et al., 2004a; Mantilla et al., 2007; Prakash et al., 1996a; Prakash et al., 1996b; Prakash et al., 1999; Prakash and Sieck, 1998; Prakash et al., 1995; Rowley et al., 2007; Sieck and Prakash, 1997). Furthermore, there are no apparent abdominal/thoracic or regional differences in fiber type distribution in the DIAm (Metzger et al., 1985; Riley and Berger, 1979; Sieck et al., 1983). Thus, using this technique a relatively large sample of NMJs could be obtained at all fiber types. Overall, ~40 motor end-plates and fibers were imaged per DIAm.

Two-dimensional projections for each motor end-plate were obtained using a maximum intensity projection algorithm available in MetaMorph software. Differences in planar areas were found to be best associated with DIAm fiber type in rats (Mantilla et al., 2004a; Mantilla et al., 2007; Prakash et al., 1996a; Prakash et al., 1996b; Prakash et al., 1999; Prakash and Sieck, 1998; Prakash et al., 1995; Rowley et al., 2007; Sieck and Prakash, 1997). DIAm fibers at selected NMJs were type-identified and their maximal XY diameter was measured at 3 separate points along their length. Of note, type I and IIa fibers had clearly defined outlines based on labeling of MyHC. Type IIx and/or IIb fibers were unlabeled in the staining protocol, but their outlines could be discerned by adjusting the dynamic range of the visualization tool in Metamorph. Motor end-plate area was determined after manually thresholding the maximal intensity projection by a pixel counting method in Metamorph.

Motor end-plate planar areas were used to calculate an index of overall NMJ complexity and to determine the relationship between NMJ size and fiber surface area. As an index of NMJ complexity, the relative planar area occupied by the motor end-plate was compared to the area defined by the major orthogonal axes of each end-plate (Fig. 6). Labeled motor end-plates were manually circumscribed by a rectangular region of interest in Metamorph. Motor end-plates were then thresholded manually to generate a binary image and the percent threshold area was obtained for each NMJ. The complexity index thus reflects branching and fragmentation in the motor end-plate area, with greater branching and fragmentation resulting in reduced relative planar area. Separately, the ratio of NMJ area to fiber surface area was calculated from the NMJ planar area and the circumferential surface area of the DIAm fiber segment that the NMJ directly overlaps (Fig. 8). The fiber surface area in this ratio was determined by the product of the estimated NMJ diameter (square root of the motor end-plate area divided by π) and the fiber circumference (based on average fiber diameter and assuming a cylinder). This index was taken to reflect the fraction of muscle fiber surface area that can be directly stimulated by the NMJ.

2.6 Photomicrograph Production

Using Fluoview software, all confocal images were stored as 12-bit multi-TIFF files. For the purposes of image production, each multicolor confocal stack was separated into individual colors (channels) in Metamorph and, if indicated in the Figure legend, a maximum intensity projection was produced using Metamorph. Individual images were exported into Adobe Photoshop (Adobe Systems Inc.; San Jose, CA) as TIFF and then down-converted into 8-bit for presentation only. Only brightness and contrast levels were adjusted linearly if needed to facilitate presentation of multiple colors.

2.7. Statistical analyses

Statistical analyses were performed using JMP software 8.0 (SAS Institute Inc, Cary, NC). Comparisons across species in ventilatory parameters, neuromuscular transmission and muscle fatigue index were conducted using a one-way analysis of variance (ANOVA). Morphological data were clustered by animal and by fiber type groups (type I and IIa vs. type IIx and/or IIb). Morphometric comparisons across fiber type groups and species were

performed using two-way ANOVA. Post hoc analyses were performed using the Tukey-Kramer honestly significant difference test when appropriate. Data were summarized as means ± SE or upper and lower 95% confidence intervals. Coefficient of determination (r^2) was also used to determine the degree of linear-correlation between variables. Statistical significance was indicated by a p value < 0.05.

3. Results

3.1. Ventilatory parameters

In awake, unrestrained adult male Sprague-Dawley rats and C57BL/6J. mice, whole body plethysmography was used to determine $\dot{V}_E$, V_T, and duration of inspiration and expiratory phases as well as total respiratory cycle duration.

3.1.1. Minute ventilation—During eupnea, $\dot{V}_E$ was 353.4 ± 8.9 ml·min^{-1} in rats and 214.3 ± 6.8 ml·min^{-1} in mice. When normalized for body weight, eupneic $\dot{V}_E$ in the mouse was disproportionately higher than the rat (Fig. 1; p<0.05, 95% CI: 1.1–1.4 ml·g^{-1}·min^{-1} in the rat, 6.9–8.6 ml·g^{-1}·min^{-1} in the mouse).

3.1.2. Tidal volume—During eupnea, V_T was 2.40 ± 0.05 ml for the rat and 0.59 ± 0.01 ml for the mouse. When normalized for body weight, V_T was disproportionately higher in the mouse compared to the rat (Fig. 1; p<0.05, 95% CI: 7.57–9.27 ml·kg^{-1} in the rat, 18.73–24.05 ml·kg^{-1} in the mouse).

3.1.3. Respiratory frequency—The frequency of breaths measured per minute was 147.2 ± 2.6 in the rat and 363.2 ± 7.7 in the mouse (p<0.05).

3.1.4. Spontaneous sighs—The frequency of spontaneous large breaths (“sighs”) was also determined. In accordance with previous studies (Mantilla et al., 2011; Mantilla et al., 2010), sighs were defined as inspiratory events that were approximately twice the volume of preceding and subsequent breaths. In the rat, sighs occurred with a frequency of 2.7 min^{-1} while awake, which is higher than the sigh frequency previously observed in anesthetized rats (0.2 min^{-1}) (Mantilla et al., 2010). No sighs were detected during quiet breathing in mice (at least 138 min of measurement in 9 mice).

3.1.5. Duty cycle—In the rat, average inspiratory duration was 0.17 ± 0.01 s compared to the total respiratory cycle duration of 0.42 ± 0.02 s during eupnea, consistent with previous reports (Mantilla et al., 2011; Mantilla et al., 2010). In the mouse, inspiratory duration was 0.08 ± 0.00 s compared to the total respiratory cycle duration of 0.17 ± 0.00 s. Thus, duty cycle was significantly higher in the mouse compared to the rat (Fig. 1; p<0.05; 95% CI: 39–44% in the rat and 45–49% in the mouse).

3.2. Fiber type proportions and differences in muscle fiber size

Fiber type in the rat and mouse DIAm could be readily distinguished based on MyHC isoform expression. Accordingly, DIAm fibers were classified as type I (expressing $MyHC_{Slow}$), type IIa (expressing $MyHC_{2A}$) or type IIx and/or IIb (expressing $MyHC_{2X}$ and/or $MyHC_{2B}$). We previously reported that in the rat DIAm, singular expression of $MyHC_{2B}$ was rarely observed (Geiger et al., 2001; Sieck et al., 2003), which justified the grouping of these fibers together with those singularly expressing $MyHC_{2X}$. In the mouse DIAm, fibers expressing $MyHC_{2B}$ were very rarely observed by immunohistochemistry (2 out of 2,271 fibers in one mouse only).

In the rat DIAm, the proportion of type I fibers was 36.2 ± 1.9 %, of type IIa fibers was 30.8 ± 1.4%, of type IIx fibers was 24.3 ± 2.0% and of type IIb fibers was 8.1 ± 1.7%. These results are consistent with previous reports (Miyata et al., 1995; Prakash et al., 2000; Zhan et al., 1997). In the mouse DIAm, the proportion of type I fibers was lower (10.7 ± 0.7%; $p<0.05$), while the proportion of type IIa fibers was higher (51.0 ± 2.0%; $p<0.05$) compared to the rat. The proportion of fatigue-resistant fibers (type I and IIa fibers) was 67% in the rat vs. 61% in the mouse ($p>0.05$). Although the proportion of type IIx fibers (38.1 ± 2.0%; $p<0.05$) was higher and type IIb fibers (0.1 ± 0.2%; $p<0.05$) was lower in the mouse DIAm, the combined proportions of type IIx and/or IIb fibers was comparable to that observed in the rat. These results in the mouse DIAm are also consistent with a previous report (LaBella et al., 1998).

In the rat DIAm, the average CSA of type I and IIa fibers were comparable (Fig. 2; $p>0.05$; 95% CI: 532–812 μm^2 and 614–786 μm^2, respectively). However, the CSA of type I and IIa fibers were ~55% smaller than type IIx and/or IIb fibers ($p<0.05$ vs. type I and IIa fibers; 95% CI: 1,592–2,296 μm^2). In the mouse DIAm, the CSA of type I and IIa fibers were also comparable ($p>0.05$; 95% CI: 379–455 μm^2 and 270–565 μm^2, respectively). Similarly, the CSA of type I and IIa fibers were ~41% smaller than type IIx fibers ($p<0.05$; 95% CI: 522–759 μm^2). Indeed, type IIx and/or IIb fibers are significantly larger than type I and IIa fibers in the rat and than all fibers in the mouse DIAm ($p<0.05$ for all comparisons). Based on the similar fiber CSA for type I and IIa fibers in both groups, subsequent analyses consider only these fiber groupings.

The relative mass contributed by type I and IIa fibers was higher in the mouse DIAm compared to the rat (type I: 8% and 22%, and type IIa: 42% and 20% in the mouse and rat, respectively).

3.3. Neuromuscular transmission failure

In both the rat and mouse DIAm, repetitive phrenic nerve stimulation clearly led to NMTF evident by reduced DIAm force generation over time (Fig. 3). The extent of neuromuscular transmission failure was significantly lower in the mouse than in the rat DIAm ($p<0.05$; 95% CI: 35–39% for the mouse vs. 55–66% for the rat). DIAm fatigability was independently assessed in separate muscle segments. The DIAm fatigue index (ratio of force after 2 min of repetitive 40-Hz stimulation to initial force) was 25.8 ± 2.1% in rats and 39.3 ± 2.0% in mice ($p<0.05$).

3.4. Fiber type differences in NMJ morphology

In both the rat and mouse DIAm, motor end-plates were clearly labeled using Alexa 488-conjugated α-bungarotoxin. In whole mount sections, DIAm fiber types were clearly identified by MyHC immunoreactivity (Fig. 4). In the DIAm, NMJs were located in a narrow band in the middle of fibers, consistent with previous reports in rats (Mantilla et al., 2004a; Mantilla et al., 2007; Prakash et al., 1999; Sieck and Prakash, 1997; Sieck et al., 1999b).

3.4.1. Motor end-plate planar areas—As previously reported in the rat DIAm (Mantilla et al., 2004a; Mantilla et al., 2007; Prakash et al., 1999; Sieck and Prakash, 1997; Sieck et al., 1999b), motor end-plate areas at type I or IIa fibers were comparable and ~43% smaller than motor end-plate areas at type IIx and/or IIb fibers (Fig. 5; $p<0.05$; 95% CI: 384–526 μm^2 for type I and IIa fibers vs. 669–932 μm^2 for type IIx and/or IIb fibers). In contrast, the planar areas of motor end-plate area at type I or IIa fibers in the mouse DIAm (95% CI: 322–379 μm^2) were similar to those at type IIx fibers (95% CI: 326–426 μm^2).

3.4.2. NMJ complexity—The relative planar area occupied by the motor end-plate was used as an index of NMJ complexity that reflects branching and fragmentation (greater branching and fragmentation results in reduced relative planar area). In the rat DIAm, the complexity of NMJs at type I or IIa fibers were comparable and ~18% less complex than those at type IIx and/or IIb (Fig. 6; $p<0.05$; 95% CI for relative NMJ planar areas: 63–73% vs. 57–64%, respectively). In the mouse DIAm, NMJ complexity was similar across fiber types ($p>0.05$; 95% CI for relative planar areas: 54–65% for type I or IIa fibers and 58–65% for type IIx fibers). The complexity of DIAm NMJs at type I and IIa fibers in the mouse was comparable to that of NMJs at type IIx and/or IIb fibers in either species.

3.4.3. Relationship between NMJ size and muscle fiber diameter—In order to evaluate the relationship between DIAm fiber dimensions and NMJ size, individual fiber diameters and motor end-plate planar areas were plotted for the DIAm of each species independent of fiber type. A significant positive correlation was found in both the rat and mouse DIAm (Fig. 7; $p<0.05$). However, in the rat DIAm the correlation was much more apparent, with an r^2 value of 0.64 for the rat compared to a much smaller r^2 value of 0.03 for the mouse. Thus, NMJ size closely relates to fiber dimensions in the rat DIAm, but not in the mouse DIAm.

3.4.4. Relationship between NMJ size and fiber surface area—The fraction of muscle fiber surface area that can be directly stimulated at the NMJ was estimated by the ratio of end-plate planar area to the circumferential surface area of the muscle fiber segment that the NMJ directly overlaps. In the rat DIAm, NMJs at type I or IIa fibers (95% CI: 15–22%) and type IIx and/or IIb fibers (95% CI: 17–23%) had similar relative overlap area (Fig. 8; $p>0.05$). In the mouse DIAm, NMJs at type I and IIa fibers displayed ~20% more relative overlap than at type IIx fibers (Fig. 8; $p<0.05$; 95% CI: 22–28% and 17–23%, respectively). Furthermore, the relative NMJ area in the mouse at DIAm type I and IIa fibers is greater than that of other NMJs of either species.

4. Discussion

The results of this study indicate that compared to the rat, the mouse had increased V_T, $\dot{V}_E$ (both normalized for body weight) and a prolonged inspiratory duty cycle during eupnea. These results suggest that the mouse DIAm has a greater activation history compared to the rat during eupneic ventilation. Consistent with these differences in ventilatory patterns, the mouse DIAm has a greater relative contribution of fatigue-resistant (type I or IIa) muscle fibers to total DIAm mass compared to the rat. Also consistent with the greater contribution of fatigue-resistant fibers, the mouse DIAm is less susceptible to neuromuscular transmission failure. However, neuromuscular transmission failure was still present in the mouse DIAm, reflecting failure predominantly at type IIx and/or IIb fibers, as previously demonstrated in rat DIAm motor units (Johnson and Sieck, 1993). In the rat DIAm, differences in NMJ morphology are associated with differences in susceptibility to neuromuscular transmission failure across fiber types. Larger and more complex motor end-plates at type IIx and/or IIb fibers consistently show greater failure rates (Ermilov et al., 2010; Mantilla et al., 2004a; Rowley et al., 2007). However, in the mouse DIAm differences in NMJ morphology were far less pronounced than in the rat. Furthermore, complexity of NMJs at all fibers in the mouse DIAm was greater than at type I or IIa fibers in the rat. These results do not support a causal relationship between fiber type differences in NMJ morphology and susceptibility to neuromuscular transmission failure.

4.1. Ventilatory parameters

All measurements were taken in awake, unrestrained adult animals. When normalized for body weight, eupneic V_T and $\dot{V}_E$ in the mouse was higher than in the rat, likely due to the greater metabolic activity of the mouse (Schmidt-Nielsen, 1970). Overall, these differences in ventilatory parameters were consistent with previous reports in either species (Mantilla et al., 2011; Mantilla et al., 2010; Shore et al., 2002; Voituron et al., 2010). During eupnea, breathing frequency was significantly higher in the mouse compared to the rat, but this was due to a disproportionate shortening of the expiratory phase causing the duty cycle to be significantly higher. Thus, to accomplish normal ventilatory behaviors, it is likely that the DIAm is more active in the mouse than in the rat.

Previous studies indicate that ventilatory parameters scale with animal size in mammals, reflecting the varying metabolic demands (Lindstedt and Schaeffer, 2002; Schmidt-Nielsen, 1970; Stahl, 1967). To accomplish normal eupneic ventilation in humans, ~10% of maximal DIAm force (normalized to maximal transdiaphragmatic pressure elicited by bilateral phrenic nerve stimulation) must be generated (Sieck, 1994). Approximately 12% of maximal DIAm force is generated during eupnea in cats compared to ~21% in rats and ~27% in hamsters (Mantilla et al., 2011; Mantilla et al., 2010; Sieck and Fournier, 1989). Consistent with such disparate ventilatory demands across species, the proportion of fatigue-resistant motor units (comprising type I and IIa fibers) is 34% in the cat compared to 65% in the rat and 54% in the hamster (Mantilla et al., 2010; Sieck, 1991; Sieck and Fournier, 1989). Although not directly measured to date, it is likely that a greater fraction of maximal DIAm force is required to sustain ventilation in the mouse. Thus, compared to the rat, the mouse is likely to have a more limited reserve capacity of the DIAm to accomplish non-ventilatory behaviors such as sighing, coughing and sneezing. These findings would be consistent with the reduced chest wall and lung compliance in the mouse compared to the rat (Leith, 1983). Furthermore, the reduced frequency of sighs in the mouse is consistent with greater DIAm force during eupnea and thus a more limited reserve capacity for DIAm activation.

Spontaneous large breaths (“sighs”) are commonly observed in humans and other mammalian species, and are thought to be a protective mechanism to avoid atelectasis. Sighs have been observed in both rats (Christon et al., 1996; Mantilla et al., 2011; Mantilla et al., 2010) and mice (Voituron et al., 2010), but the frequency of spontaneous sighs was much lower in the mouse compared to the rat. Indeed, in the awake, unrestrained mouse, sighs were not detected in the present study. This may relate to the definition of a sigh as inspiratory events that were approximately twice the volume of preceding and subsequent breaths, but this definition does not appear to be too stringent for the mouse (Voituron et al., 2010). Another reason sighs were not detected in the mouse could be the experimental condition, with studies examining anesthetized (Mantilla et al., 2011; Mantilla et al., 2010) and awake unrestrained animals (present study). Indeed, we found that in awake rats the frequency of sighs was substantially higher than that previously observed in anesthetized rats.

4.2. Fiber type proportions and differences in muscle fiber size

The fiber proportions observed in the present study are consistent with previous reports in the rat (Miyata et al., 1995; Prakash et al., 2000; Zhan et al., 1997) and mouse DIAm (LaBella et al., 1998).Compared to the rat, the proportion of type IIx fibers was higher in the mouse DIAm. Type IIb fibers were rarely observed in the mouse DIAm (0.1%). However, type IIb fibers were previously reported (6.2%) in the mouse DIAm (Agbulut et al., 2003). Regardless, the combined proportion of type IIx and/or IIb fibers was comparable between rats and mice. Type IIx and/or IIb fibers in the rat DIAm are significantly larger in CSA than type I and IIa fibers, and than all fibers in the mouse DIAm. Differences in fiber CSA were

far less pronounced in the mouse compared to the rat DIAm. Accordingly, type I or IIa fibers comprise a larger portion of total DIAm mass in the mouse. These results suggest that the relative contribution of fatigue-resistant muscle fibers to total DIAm mass scales in accordance to ventilatory demands. In addition, a reduced relative contribution of type IIx (and/or IIb) muscle fibers to DIAm mass is consistent with a more limited reserve capacity to accomplish non-ventilatory behaviors in the mouse compared to the rat.

4.3. Neuromuscular transmission failure

In both the mouse and rat DIAm, repetitive phrenic nerve stimulation clearly led to neuromuscular transmission failure evident by reduced DIAm force generation over time. The extent of neuromuscular transmission failure was significantly lower in the mouse than in the rat DIAm. The lower susceptibility of the mouse DIAm to neuromuscular transmission failure is consistent with the reduced portion of DIAm mass comprised by type IIx and/or IIb fibers. Motor units comprising type IIx and/or IIb fibers in the rat DIAm are more susceptible to failure than those comprising type I or IIa fibers (Johnson and Sieck, 1993; Sieck and Prakash, 1995).

Significant functional differences exist across motor unit types, including at the NMJ. For instance, the safety factor for neuromuscular transmission is higher at type IIx and/or IIb fibers compared to type I or IIa fibers in the rat (Ermilov et al., 2007; Wood and Slater, 1997, 2001). However, quantal release at type IIx and/or IIb fibers declines far more rapidly with repetitive stimulation than at type I or IIa fibers (Reid et al., 1999; Rowley et al., 2007). Previous studies support fiber type differences in NMJ structure and function (Banker et al., 1983; Fahim et al., 1984; Mantilla et al., 2004a; Prakash et al., 1996a; Prakash et al., 1999; Rowley et al., 2007; Sieck et al., 1999b).

4.4. Fiber type differences in NMJ morphology

In agreement with previous reports in the rat DIAm (Mantilla et al., 2004a; Prakash et al., 1996b; Rowley et al., 2007; Sieck and Prakash, 1997), NMJs at type I and IIa fibers are smaller and less complex compared to NMJs at type IIx and/or IIb fibers. In the mouse DIAm, there were no significant fiber type differences in NMJ morphology. Only one strain of two commonly used species was used in the present study. Clearly, there may be strain differences within each of these species. Regardless, there were differences in NMJ morphology (size, complexity and branching) and relative NMJ areas (as a ratio of muscle fiber surface area) which may contribute to differences in susceptibility to neuromuscular transmission failure, yet neuromuscular transmission failure was still observed in both species.

Neuromuscular transmission failure may depend on branch-point failure or postsynaptic properties related to fiber size (Sieck and Prakash, 1995). In this sense, NMJs at type I or IIa fibers are less complex (i.e., fragmented) in the adult rat DIAm. However, DIAm NMJs at type IIx and/or IIb fibers and mouse NMJs show considerably greater branching and complexity than NMJs at type I or IIa fibers in the rat DIAm. Thus, NMJ complexity in the mouse is similar to that at rat NMJs that display considerably greater transmission failure (Ermilov et al., 2007). NMJ size does relate to muscle fiber size, but the strength of this relationship varies across rodent species. A positive correlation between NMJ size and DIAm fiber diameter was present in both rats and mice, although it was much more apparent in the rat (r^2=0.64 vs. r^2=0.03 in the rat and mouse, respectively). Importantly, the relative areas of motor end-plates (normalized to muscle fiber surface area) at type I or IIa fibers in the mouse DIAm are larger than type IIx and/or IIb fibers, and larger than in rat DIAm fibers. Although this difference does not reflect a common characteristic across these strains

of rodent species, increased relative motor end-plate area would likely improve neuromuscular transmission in the mouse.

4.5. Determinants of morphological diversity across fiber types

Differences in the motor end-plate morphology across fiber types may reflect differences in fiber size, activation history, loading conditions or genetic pre-programming. Based on the results of the present study, morphological differences are not accounted for by differences in DIAm fiber size. Neuromuscular characteristics may reflect differences in neural influence which relate to motor unit properties or activity (Reid et al., 2003; Waerhaug and Lomo, 1994). Recruitment of DIAm motor units varies across ventilatory and non-ventilatory behaviors (Fournier and Sieck, 1988; Mantilla et al., 2010; Sieck, 1991, 1994; Sieck and Fournier, 1989). In the rat DIAm, motor units comprising type I or IIa fibers can account for forces generated during ventilatory behaviors. Only during more forceful behaviors such as sighing, sneezing or coughing do forces generated by the DIAm necessitate recruitment of motor units comprising type IIx and/or IIb fibers (Mantilla et al., 2010). To date, there is no such information available for the mouse. However, it is possible that some motor unit type differences reflect differences in activation patterns even within a single, very active muscle such as the DIAm. It is worth noting that the frequency of relatively large breaths (“sighs”) is much greater in rats than in mice. This may reflect recruitment of motor units comprising type IIx fibers in the mouse during eupneic behaviors, consistent with an overall greater activation history in the mouse compared to the rat. Therefore, it is likely that morphological differences at the NMJ reflect motor neuron properties independent of actual activity levels, but the effect of discharge rates or patterns cannot be excluded. Presently, there is scant information regarding DIAm motor unit discharge rates in the mouse (Lee and Fuller, 2011). Although the DIAm load associated with the overall compliance of the respiratory system differs between mice and rats, both chest wall and lung compliance scale with body mass (Leith, 1983). In addition, the DIAm is not gravitationally loaded in either species (Rowley et al., 2005); thus, it is unlikely that differences in loading conditions contribute to differences in NMJ morphology across fiber types in these rodent strains.

4.6. Research Implications

The scaling of ventilatory parameters across these two rodent species indicates that recruitment of a greater fraction of the DIAm in the mouse is required to sustain eupnea compared to the rat. This conclusion is supported by the greater relative contribution of fatigue resistant type I and IIa fibers to DIAm mass in the mouse, and the reduced susceptibility of the mouse DIAm to neuromuscular transmission failure. In addition, fiber type differences in NMJ morphology presented in the rat DIAm were not as apparent in the mouse, which may also reflect the greater relative activity of the mouse DIAm. These differences across two closely related species suggest that extrapolation of findings in rodents to humans must be done cautiously. There is considerable evidence to indicate that the reserve capacity of the human DIAm is substantially larger than either of these rodent species (Sieck, 1991, 1995). Thus, pathophysiological conditions that lead to DIAm fiber atrophy may not be reflected by alterations in ventilatory capacity (Mantilla and Sieck, 2011; Sieck and Fournier, 1989; Sieck and Mantilla, 2008), and far less information is available regarding non-ventilatory behaviors that utilize this DIAm reserve capacity. Limited data suggest that differences in DIAm fiber CSA are not as pronounced in humans, but these are largely based on small biopsy samples (Levine et al., 2003; Ottenheijm et al., 2005; Welvaart et al., 2011). Such studies have drawn sometimes conflicting conclusions regarding changes in fiber CSA under pathophysiological conditions. Unfortunately, to the best of our knowledge there has been no systematic examination of the relative contributions of different fiber types to human DIAm mass under any condition.

Highlights

>Diaphragm muscle in mice has a greater activation history than rats. >Susceptibility to neuromuscular transmission failure is less in mice than rats. >Fatigue-resistant fibers contribute to a greater fraction of muscle mass in mice. >Rats, but not mice, show fiber type differences in neuromuscular junction morphology. >Functional differences across species are not reflected in neuromuscular morphology.

Acknowledgments

Supported by NIH grants HL096750, AR051173, and a Career Development Award from Mayo Clinic.

References

Agbulut O, Noirez P, Beaumont F, Butler-Browne G. Myosin heavy chain isoforms in postnatal muscle development of mice. Biol. Cell. 2003; 95:399–406. [PubMed: 14519557]

Aldrich TK, Shander A, Chaudhry I, Nagashima H. Fatigue of isolated rat diaphragm: role of impaired neuromuscular transmission. J. Appl. Physiol. 1986; 61:1077–1083. [PubMed: 3019989]

Banker BQ, Kelly SS, Robbins N. Neuromuscular transmission and correlative morphology in young and old mice. J. Physiol. 1983; 339:355–377. [PubMed: 6310088]

Christon J, Carley DW, Monti D, Radulovacki M. Effects of inspired gas on sleep-related apnea in the rat. J. Appl. Physiol. 1996; 80:2102–2107. [PubMed: 8806919]

Enad JG, Fournier M, Sieck GC. Oxidative capacity and capillary density of diaphragm motor units. J. Appl. Physiol. 1989; 67:620–627. [PubMed: 2529236]

Ermilov LG, Mantilla CB, Rowley KL, Sieck GC. Safety factor for neuromuscular transmission at type-identified diaphragm fibers. Muscle Nerve. 2007; 35:800–803. [PubMed: 17286272]

Ermilov LG, Pulido JN, Atchison FW, Zhan WZ, Ereth MH, Sieck GC, Mantilla CB. Impairment of diaphragm muscle force and neuromuscular transmission after normothermic cardiopulmonary bypass: effect of low dose inhaled CO. Am. J. Physiol. Regul. Integr. Comp. Physiol. 2010; 298:R784–R789. [PubMed: 20089713]

Fahim MA, Holley JA, Robbins N. Topographic comparison of neuromuscular junctions in mouse slow and fast twitch muscles. Neurosci. 1984; 13:227–235.

Fournier M, Alula M, Sieck GC. Neuromuscular transmission failure during postnatal development. Neurosci. Lett. 1991; 125:34–36. [PubMed: 1649983]

Fournier M, Sieck GC. Mechanical properties of muscle units in the cat diaphragm. J. Neurophysiol. 1988; 59:1055–1066. [PubMed: 3367195]

Geiger PC, Cody MJ, Macken RL, Bayrd ME, Sieck GC. Mechanisms underlying increased force generation by rat diaphragm muscle fibers during development. J. Appl. Physiol. 2001; 90:380–388. [PubMed: 11133931]

Johnson BD, Sieck GC. Differential susceptibility of diaphragm muscle fibers to neuromuscular transmission failure. J. Appl. Physiol. 1993; 75:341–348. [PubMed: 8397179]

Kuei JH, Shadmehr R, Sieck GC. Relative contribution of neurotransmission failure to diaphragm fatigue. J. Appl. Physiol. 1990; 68:174–180. [PubMed: 2155900]

Kugelberg E, Lindegren B. Transmission and contraction fatigue of rat motor units in relation to succinate dehydrogenase activity of motor unit fibres. J. Physiol. 1979; 288:285–300. [PubMed: 224167]

LaBella JJ, Daood MJ, Koretsky AP, Roman BB, Sieck GC, Wieringa B, Watchko JF. Absence of myofibrillar creatine kinase and diaphragm isometric function during repetitive activation. J. Appl. Physiol. 1998; 84:1166–1173. [PubMed: 9516180]

Lee KZ, Fuller DD. Neural control of phrenic motoneuron discharge. Respir. Physiol. Neurobiol. 2011

Leith DE. Comparative mammalian respiratory mechanics. Am. Rev. Respir. Dis. 1983; 128:S77–S82. [PubMed: 6881717]

Levine S, Nguyen T, Kaiser LR, Rubinstein NA, Maislin G, Gregory C, Rome LC, Dudley GA, Sieck GC, Shrager JB. Human diaphragm remodeling associated with chronic obstructive pulmonary disease: clinical implications. Am. J. Respir. Crit. Care Med. 2003; 168:706–713. [PubMed: 12857719]

Lewis MI, Sieck GC, Fournier M, Belman MJ. Effect of nutritional deprivation on diaphragm contractility and muscle fiber size. J. Appl. Physiol. 1986; 60:596–603. [PubMed: 3949661]

Lindstedt SL, Schaeffer PJ. Use of allometry in predicting anatomical and physiological parameters of mammals. Lab Anim. 2002; 36:1–19. [PubMed: 11833526]

Mantilla CB, Rowley KL, Fahim MA, Zhan WZ, Sieck GC. Synaptic vesicle cycling at type-identified diaphragm neuromuscular junctions. Muscle Nerve. 2004a; 30:774–783. [PubMed: 15478121]

Mantilla CB, Rowley KL, Zhan WZ, Fahim MA, Sieck GC. Synaptic vesicle pools at diaphragm neuromuscular junctions vary with motoneuron soma, not axon terminal, inactivity. Neurosci. 2007; 146:178–189.

Mantilla CB, Seven YB, Hurtado-Palomino JN, Zhan WZ, Sieck GC. Chronic assessment of diaphragm muscle EMG activity across motor behaviors. Respir. Physiol. Neurobiol. 2011; 177:176–182. [PubMed: 21414423]

Mantilla CB, Seven YB, Zhan WZ, Sieck GC. Diaphragm motor unit recruitment in rats. Respir. Physiol. Neurobiol. 2010; 173:101–106. [PubMed: 20620243]

Mantilla CB, Sieck GC. Phrenic motor unit recruitment during ventilatory and non-ventilatory behaviors. Respir. Physiol. Neurobiol. 2011

Mantilla CB, Zhan WZ, Sieck GC. Neurotrophins improve neuromuscular transmission in the adult rat diaphragm. Muscle Nerve. 2004b; 29:381–386. [PubMed: 14981737]

Metzger JM, Scheidt KB, Fitts RH. Histochemical and physiological characteristics of the rat diaphragm. J. Appl. Physiol. 1985; 58:1085–1091. [PubMed: 3988665]

Miyata H, Zhan WZ, Prakash YS, Sieck GC. Myoneural interactions affect diaphragm muscle adaptations to inactivity. J. Appl. Physiol. 1995; 79:1640–1649. [PubMed: 8594024]

Ottenheijm CA, Heunks LM, Sieck GC, Zhan WZ, Jansen SM, Degens H, de Boo T, Dekhuijzen PN. Diaphragm dysfunction in chronic obstructive pulmonary disease. Am. J. Respir. Crit. Care Med. 2005; 172:200–205. [PubMed: 15849324]

Prakash YS, Gosselin LE, Zhan WZ, Sieck GC. Alterations of diaphragm neuromuscular junctions with hypothyroidism. J. Appl. Physiol. 1996a; 81:1240–1248. [PubMed: 8889759]

Prakash YS, Mantilla CB, Zhan WZ, Smithson KG, Sieck GC. Phrenic motoneuron morphology during rapid diaphragm muscle growth. J. Appl. Physiol. 2000; 89:563–572. [PubMed: 10926639]

Prakash YS, Miller SM, Huang M, Sieck GC. Morphology of diaphragm neuromuscular junctions on different fibre types. J. Neurocytol. 1996b; 25:88–100. [PubMed: 8699198]

Prakash YS, Miyata H, Zhan WZ, Sieck GC. Inactivity-induced remodeling of neuromuscular junctions in rat diaphragmatic muscle. Muscle Nerve. 1999; 22:307–319. [PubMed: 10086891]

Prakash YS, Sieck GC. Age-related remodeling of neuromuscular junctions on type-identified diaphragm fibers. Muscle Nerve. 1998; 21:887–895. [PubMed: 9626248]

Prakash YS, Smithson KG, Sieck GC. Measurements of motoneuron somal volumes using laser confocal microscopy: comparisons with shape-based stereological estimations. Neuroimage. 1993; 1:95–107. [PubMed: 9343561]

Prakash YS, Smithson KG, Sieck GC. Application of the Cavalieri principle in volume estimation using laser confocal microscopy. Neuroimage. 1994; 1:325–333. [PubMed: 9343582]

Prakash YS, Zhan WZ, Miyata H, Sieck GC. Adaptations of diaphragm neuromuscular junction following inactivity. Acta. Anat. (Basel). 1995; 154:147–161. [PubMed: 8722515]

Reid B, Martinov VN, Nja A, Lomo T, Bewick GS. Activity-dependent plasticity of transmitter release from nerve terminals in rat fast and slow muscles. J. Neurosci. 2003; 23:9340–9348. [PubMed: 14561861]

Reid B, Slater CR, Bewick GS. Synaptic vesicle dynamics in rat fast and slow motor nerve terminals. J. Neurosci. 1999; 19:2511–2521. [PubMed: 10087065]

Riley DA, Berger AJ. A regional histochemical and electromyographic analysis of the cat respiratory diaphragm. Exp. Neurol. 1979; 66:636–649. [PubMed: 488243]

Rowley KL, Mantilla CB, Ermilov LG, Sieck GC. Synaptic vesicle distribution and release at rat diaphragm neuromuscular junctions. J. Neurophysiol. 2007; 98:478–487. [PubMed: 17493926]

Rowley KL, Mantilla CB, Sieck GC. Respiratory muscle plasticity. Respir. Physiol. Neurobiol. 2005; 147:235–251. [PubMed: 15871925]

Schmidt-Nielsen K. Energy metabolism, body size, and problems of scaling. Fed. Proc. 1970; 29:1524–1532. [PubMed: 5459901]

Shore SA, Johnston RA, Schwartzman IN, Chism D, Krishna Murthy GG. Ozone-induced airway hyperresponsiveness is reduced in immature mice. J. Appl. Physiol. 2002; 92:1019–1028. [PubMed: 11842035]

Sieck GC. Diaphragm muscle: structural and functional organization. Clin. Chest. Med. 1988; 9:195–210. [PubMed: 3292123]

Sieck GC. Neural control of the inspiratory pump. NIPS. 1991; 6:260–264.

Sieck GC. Physiological effects of diaphragm muscle denervation and disuse. Clin. Chest. Med. 1994; 15:641–659. [PubMed: 7867280]

Sieck, GC. Organization and recruitment of diaphragm motor units. In: Roussos, C., editor. The Thorax. Second ed.. New York, NY: Marcel Dekker; 1995. p. 783-820.

Sieck GC, Blanco CE. Postnatal changes in the distribution of succinate dehydrogenase activities among diaphragm muscle fibers. Pediatr. Res. 1991; 29:586–593. [PubMed: 1830959]

Sieck GC, Fournier M. Diaphragm motor unit recruitment during ventilatory and nonventilatory behaviors. J. Appl. Physiol. 1989; 66:2539–2545. [PubMed: 2745316]

Sieck GC, Fournier M, Enad JG. Fiber type composition of muscle units in the cat diaphragm. Neurosci.. Lett. 1989a; 97:29–34. [PubMed: 2521928]

Sieck GC, Fournier M, Prakash YS, Blanco CE. Myosin phenotype and SDH enzyme variability among motor unit fibers. J. Appl. Physiol. 1996; 80:2179–2189. [PubMed: 8806928]

Sieck GC, Lewis MI, Blanco CE. Effects of undernutrition on diaphragm fiber size, SDH activity, and fatigue resistance. J. Appl. Physiol. 1989b; 66:2196–2205. [PubMed: 2745285]

Sieck GC, Mantilla CB. Effect of mechanical ventilation on the diaphragm. N. Engl. J. Med. 2008; 358:1392–1394. [PubMed: 18367743]

Sieck GC, Mantilla CB, Prakash YS. Volume measurements in confocal microscopy. Methods Enzymol. 1999a; 307:296–315. [PubMed: 10506980]

Sieck GC, Prakash YS. Fatigue at the neuromuscular junction. Branch point vs. presynaptic vs. postsynaptic mechanisms. Adv. Exp. Med. Biol. 1995; 384:83–100. [PubMed: 8585479]

Sieck GC, Prakash YS. Morphological adaptations of neuromuscular junctions depend on fiber type. Can. J. Appl. Physiol. 1997; 22:197–230. [PubMed: 9189302]

Sieck GC, Prakash YS, Han YS, Fang YH, Geiger PC, Zhan WZ. Changes in actomyosin ATP consumption rate in rat diaphragm muscle fibers during postnatal development. J. Appl. Physiol. 2003; 94:1896–1902. [PubMed: 12562672]

Sieck GC, Roy RR, Powell P, Blanco C, Edgerton VR, Harper RM. Muscle fiber type distribution and architecture of the cat diaphragm. J. Appl. Physiol. 1983; 55:1386–1392. [PubMed: 6643176]

Sieck GC, Van Balkom RH, Prakash YS, Zhan WZ, Dekhuijzen PN. Corticosteroid effects on diaphragm neuromuscular junctions. J. Appl. Physiol. 1999b; 86:114–122. [PubMed: 9887121]

Stahl WR. Scaling of respiratory variables in mammals. J. Appl. Physiol. 1967; 22:453–460. [PubMed: 6020227]

Voituron N, Zanella S, Menuet C, Lajard AM, Dutschmann M, Hilaire G. Early abnormalities of post-sigh breathing in a mouse model of Rett syndrome. Respir. Physiol. Neurobiol. 2010; 170:173–182. [PubMed: 20040383]

Waerhaug O, Lomo T. Factors causing different properties at neuromuscular junctions in fast and slow rat skeletal muscles. Anat. Embryol. (Berl.). 1994; 190:113–125. [PubMed: 7818085]

Welvaart WN, Paul MA, van Hees HW, Stienen GJ, Niessen JW, de Man FS, Sieck GC, Vonk-Noordegraaf A, Ottenheijm CA. Diaphragm muscle fiber function and structure in humans with hemidiaphragm paralysis. Am. J. Physiol. Lung Cell Mol. Physiol. 2011; 301:L228–L235. [PubMed: 21622847]

Wood SJ, Slater CR. The contribution of postsynaptic folds to the safety factor for neuromuscular transmission in rat fast- and slow-twitch muscles. J. Physiol. 1997; 500:165–176. [PubMed: 9097941]

Wood SJ, Slater CR. Safety factor at the neuromuscular junction. Prog. Neurobiol. 2001; 64:393–429. [PubMed: 11275359]

Zhan WZ, Miyata H, Prakash YS, Sieck GC. Metabolic and phenotypic adaptations of diaphragm muscle fibers with inactivation. J. Appl. Physiol. 1997; 82:1145–1153. [PubMed: 9104851]

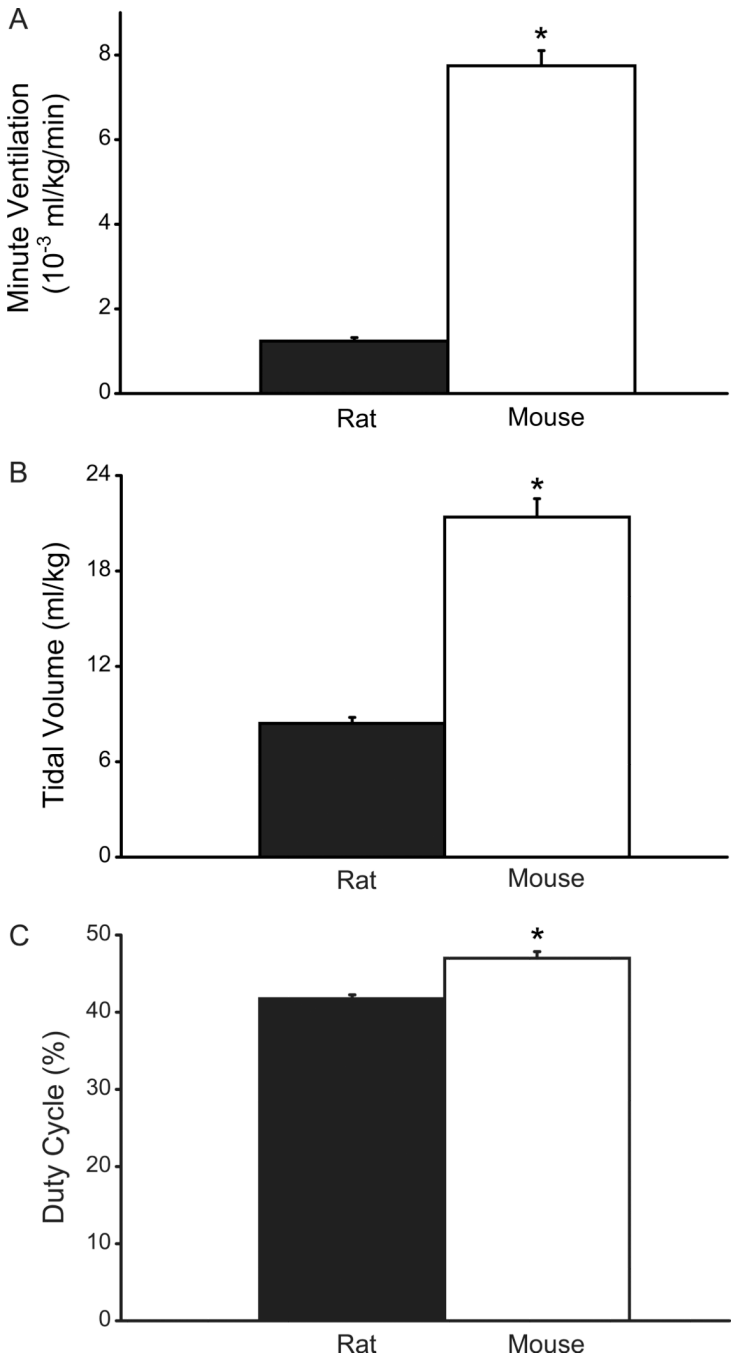

Fig. 1.

Ventilatory parameters in adult rats (n=10) and mice (n=9) measured in awake, unrestrained animals using whole body plethysmography. **A**. Minute ventilation ($\times 10^{-3}$ ml/kg/min); **B**. tidal volume (ml/kg); and, **C**. duty cycle (percent inspiratory time out of total cycle time). All ventilatory parameters were significantly greater in the adult mouse compared to the rat even when adjusted for differences in body weight. Data are mean (± SE). *, denotes statistically significant difference compared to the rat ($p<0.05$).

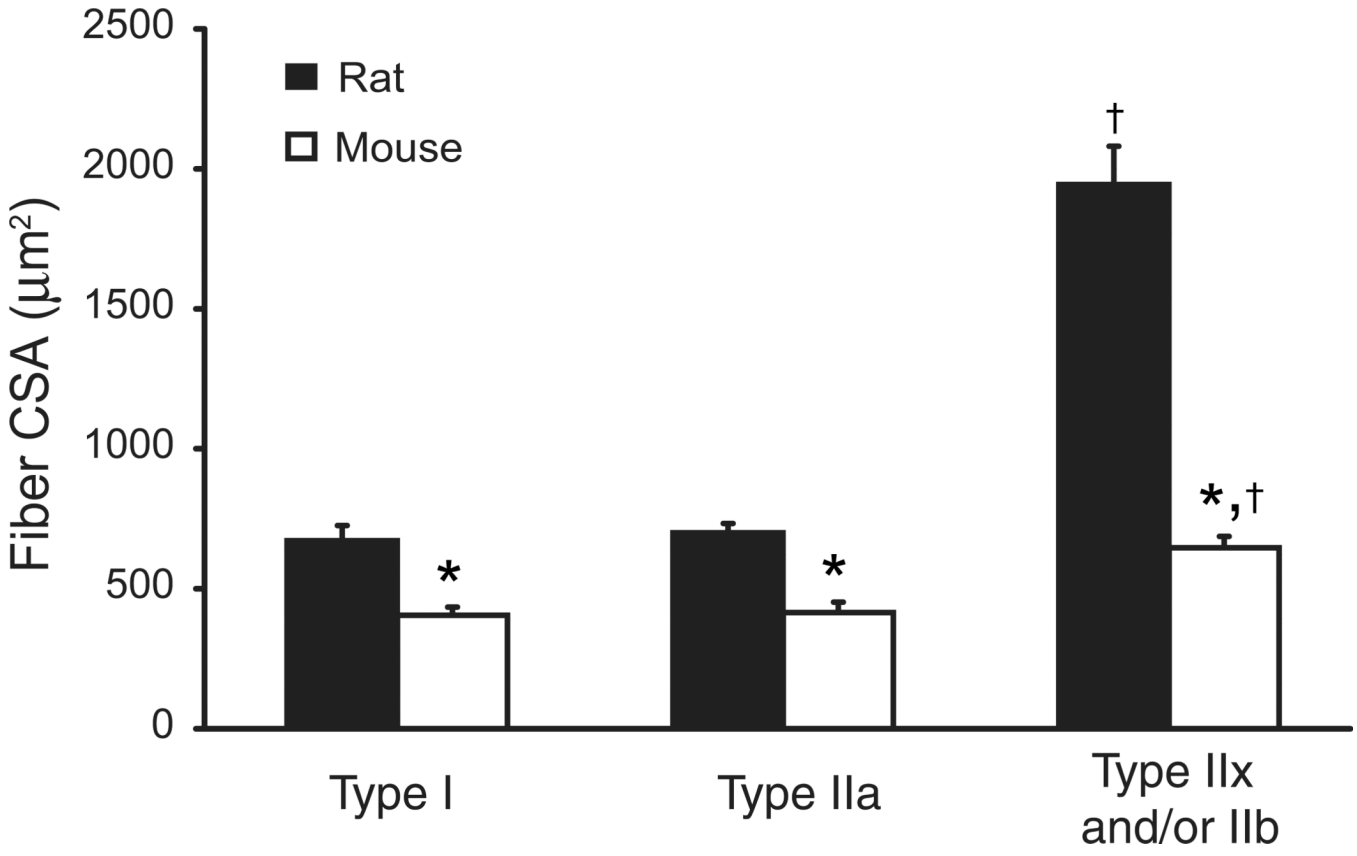

Fig. 2.

Cross-sectional area (CSA) of adult rat and mouse diaphragm muscle (DIAm) fibers (n=6 animals of each species for all morphological measurements). DIAm fiber classification is based on myosin heavy chain (MyHC) isoform expression (type I, type IIa and type IIx and/or IIb). Note differences across species in the relative size of muscle fibers. In both species, fiber CSA was greater at type IIx and/or IIb fibers compared to type I or IIa fibers. Data are mean (± SE) muscle fiber CSA (μm^2). *, denotes statistically significant difference compared to rat for the same fiber type; †, denotes statistically significant difference vs. type I or IIa fibers of the same species.

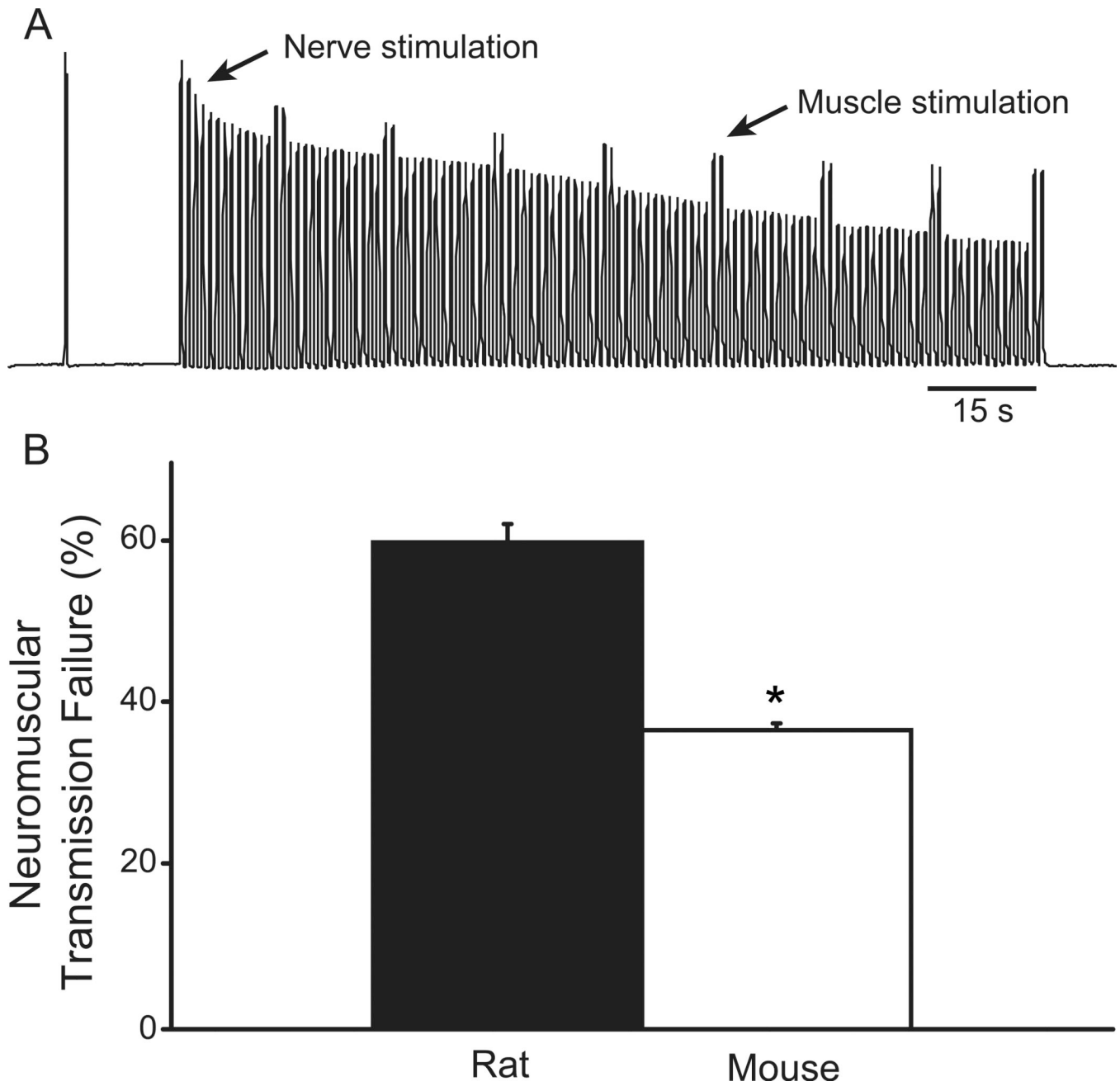

Fig. 3.

Contribution of neuromuscular transmission failure to DIAm fatigue in the rat and mouse. **A**. Representative tracing of force developed by the DIAm from an adult mouse that was electrically stimulated (40 Hz in 330-ms trains) indirectly via the phrenic nerve (every 1 s) and directly via plate electrodes (every 15 s). The DIAm generates decreasing force with repetitive stimulation, indicative of fatigue. The difference in the relative force elicited by direct and nerve (indirect) stimulation reflects neuromuscular transmission failure (see Methods). Neuromuscular transmission failure was determined following 2-min of repetitive stimulation. **B**. Mean (±SE) neuromuscular transmission failure in adult rat (n=6) and mouse (n=8) phrenic nerve-diaphragm muscle preparations. Neuromuscular transmission failure

was significantly lower in the mouse compared to the rat. *, denotes statistically significant difference compared to the rat.

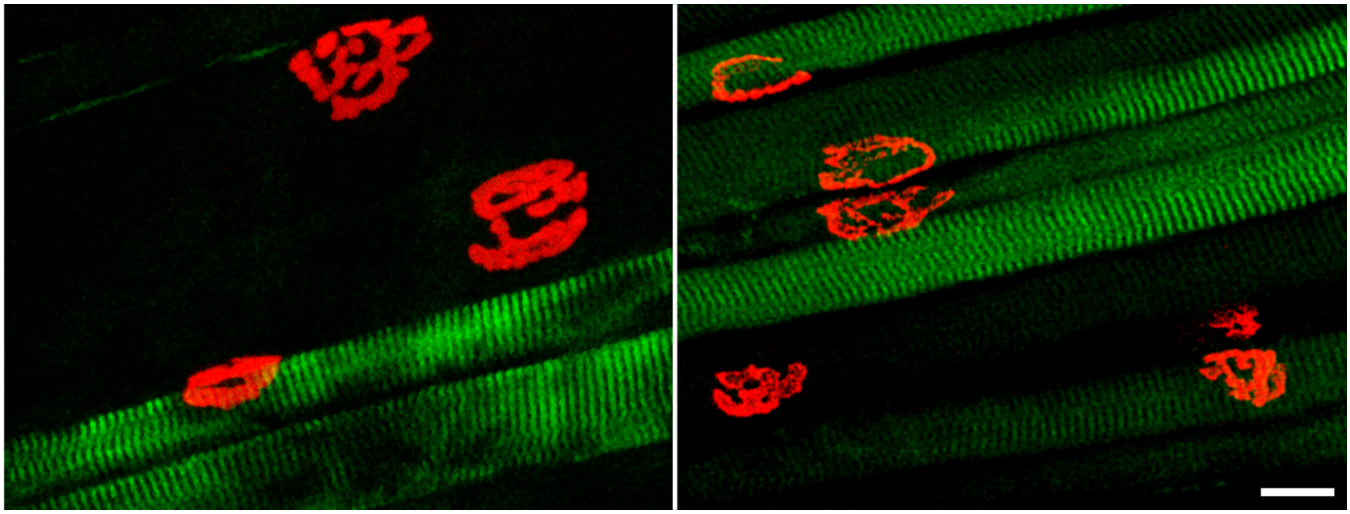

Fig. 4.

Motor end-plates at type-identified rat and mouse DIAm fibers. Representative confocal photomicrographs of neuromuscular junctions (NMJ) and type-identified DIAm fibers. Motor end-plates were labeled with Alexa 488-conjugated α-bungarotoxin and fiber types were identified by immunoreactivity to $MyHC_{Slow}$ or $MyHC_{2A}$ isoforms (type I or IIa fibers). Unlabeled fibers express $MyHC_{2X}$ and/or $MyHC_{2B}$ isoforms (type IIx and/or IIb fibers; see Methods). Maximum intensity projections showing significant differences in NMJ size, NMJ morphology and fiber dimensions across fiber types in the rat DIAm (left) but more similar NMJ size and morphology across fibers types in the mouse DIAm (right). Bar, 20 μm.

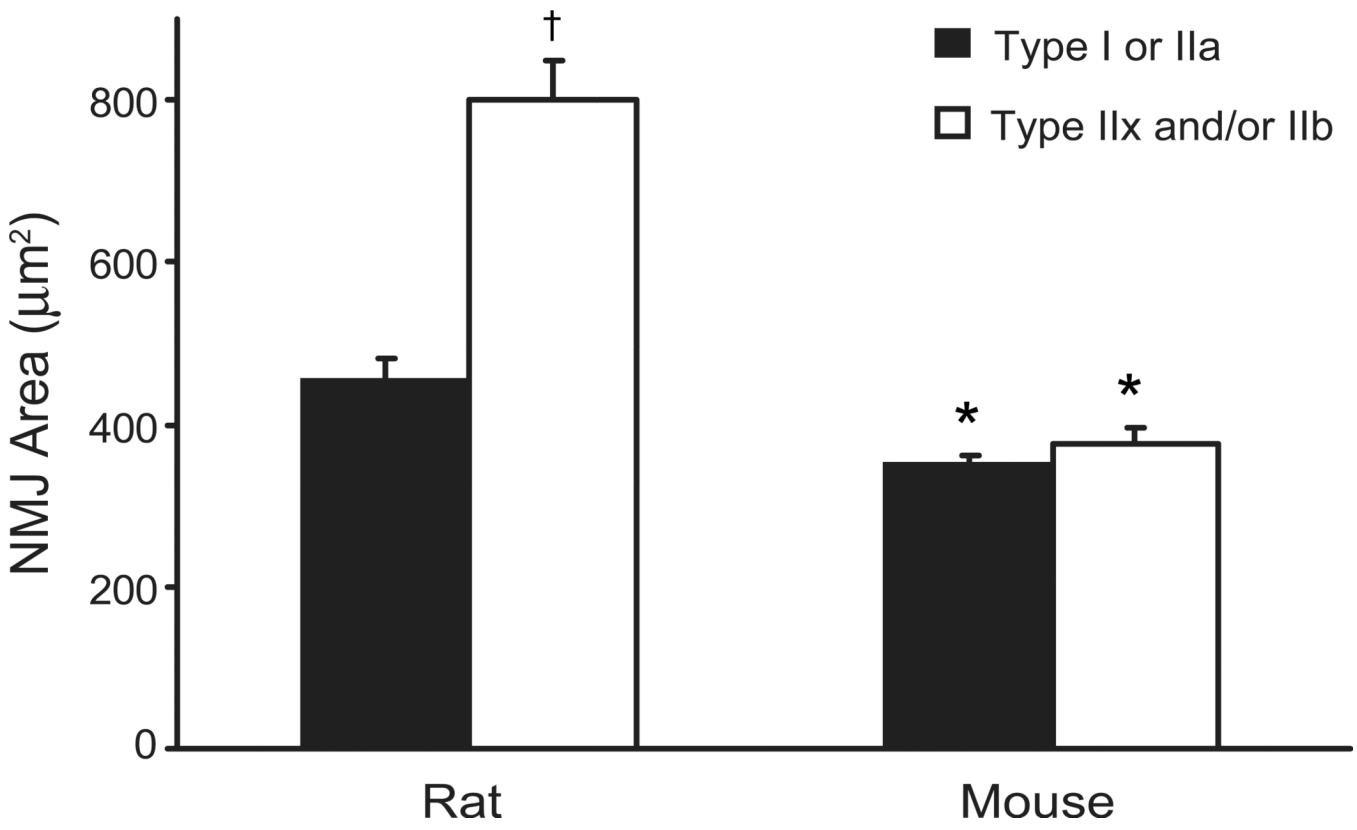

Fig. 5.

Motor end-plate area across DIAm fibers of different type. Mean (± SE) planar area (μm^2) at type-identified DIAm fibers across species. NMJ area is significantly larger at type IIx and/or IIb fibers in the rat, but not in the mouse DIAm, compared to type I or IIa fibers. *, denotes statistically significant difference compared to rat for the same fiber type; †, denotes statistically significant difference vs. type I or IIa fibers of the same species.

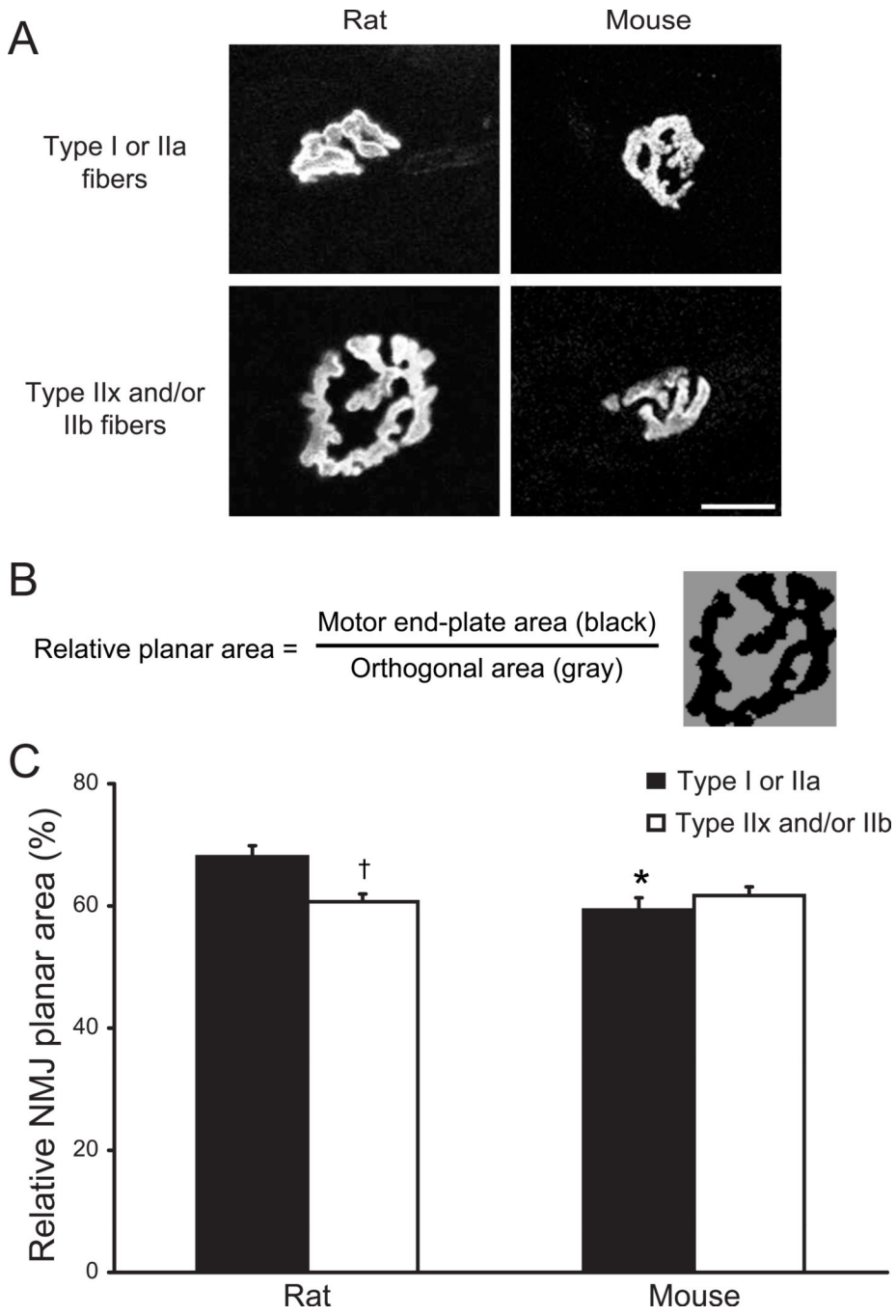

Fig. 6.

Complexity of NMJ morphology in the DIAm of adult rats and mice. **A**. Representative confocal photomicrographs of DIAm NMJs at different fibers types. Maximum intensity projections show differences in NMJ complexity across fiber types in the rat DIAm (left panels) and more similar NMJ complexity across fiber types in the mouse DIAm (right panels). Bar, 20 μm. **B**. As a quantitative index of NMJ complexity, the relative planar area occupied by the motor end-plate was compared to the area defined by the major orthogonal axes of each end-plate (see Methods). Thus, this index reflects branching and fragmentation in the motor end-plate area (greater fragmentation results in reduced relative planar area). **C**. Relative NMJ planar area (%) for type-identified DIAm NMJs of rats and mice. Note

quantitative differences in complexity across fiber types in DIAm NMJs of the adult rat, but not mouse. Data are mean (± SE). *, denotes statistically significant difference compared to rat for the same fiber type; †, denotes statistically significant difference vs. type I or IIa fibers of the same species.

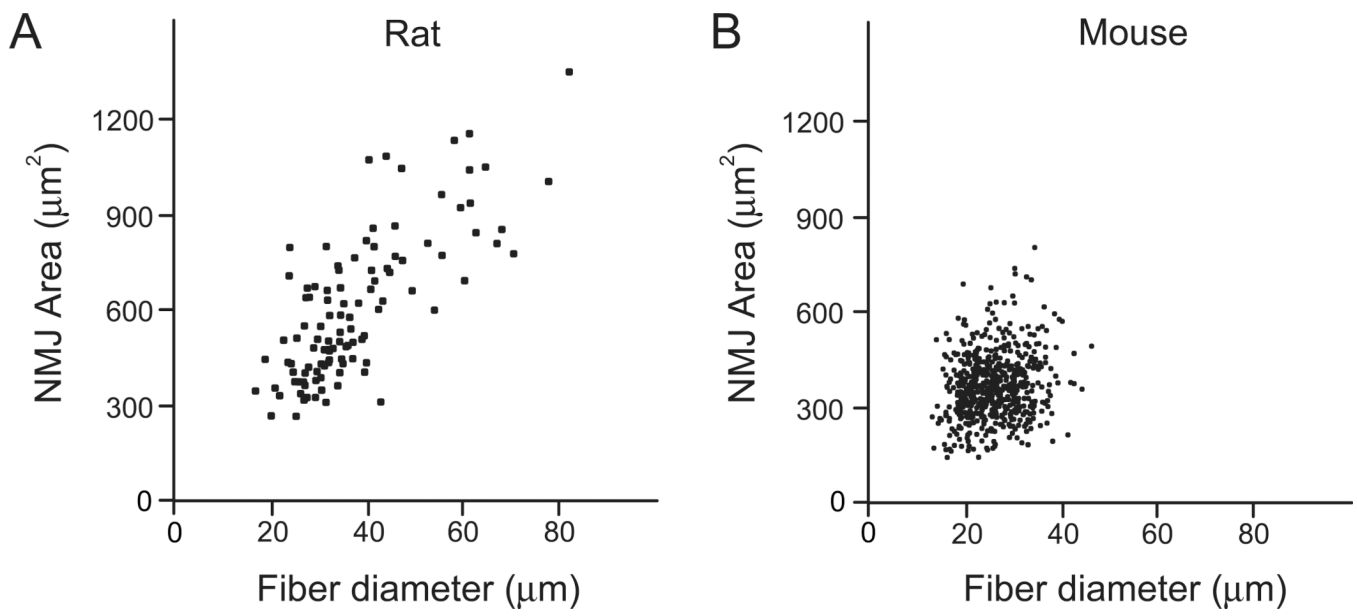

Fig. 7.

Correlation between NMJ area and fiber diameter in the adult rat (**A**) and mouse DIAm (**B**). Motor end-plate planar area (μm^2) was plotted against muscle fiber diameter (μm) for each DIAm NMJ. A positive correlation was found in both species ($p<0.05$). However, the correlation was much stronger in the rat than in the mouse ($r^2=0.64$ vs. $r^2=0.03$, respectively).

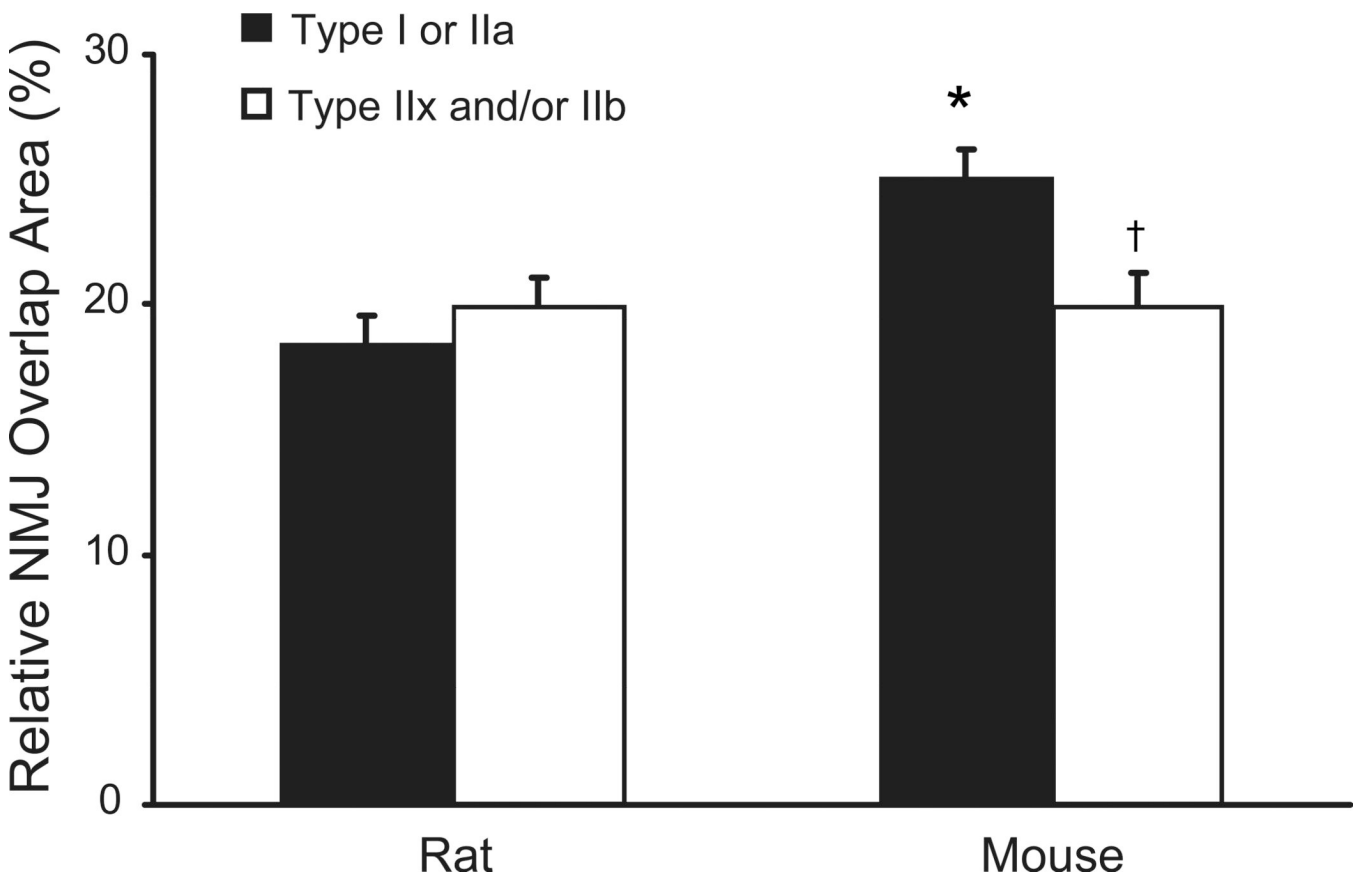

Fig. 8.

Relationship between motor end-plate area and fiber surface area in the adult DIAm of rats and mice. The relative overlap area, i.e., area covered by a motor end-plate per DIAm fiber surface area, was calculated as the ratio of NMJ. area to the circumferential surface area for the fiber segment that the NMJ. directly overlaps. There were no fiber type differences in the relative overlap area in the rat, but mouse type I and IIa fibers had a significantly higher overlap area compared to type IIx fibers. Data are mean (± SE). *, denotes statistically significant difference compared to rat for the same fiber type; †, denotes statistically significant difference vs. type I or IIa fibers of the same species.